Covariation Informed Graph Slepians for Motor Imagery Decoding

Kostas Georgiadis, *Graduate Student Member, IEEE*, Dimitrios A. Adamos, *Member, IEEE*, Spiros Nikolopoulos, Nikos Laskaris, and Ioannis Kompatsiaris, *Senior Member, IEEE*

***Abstract*— Graph signal processing (GSP) provides signal analytic tools for data defined in irregular domains, as is the case of non-invasive electroencephalography (EEG). In this work, the recently introduced technique of *Graph Slepian functions* is exploited for the robust decoding of motor imagery (MI) brain activity. The particular technique builds over the concept of graph Fourier transform (GFT) and provides additional flexibility in the subsequent data analysis by incorporating domain knowledge. Based on contrastive learning, we introduce an algorithmic pipeline that attains a data driven and subject specific design of Graph Slepian functions. These functions, by incorporating both the topology of the sensor array and the empirical evidence about the differential functional covariation, act as spatial filters that enhance the information conveyed by the multichannel signal and specifically relates to the participant's intention. The proposed technique for crafting Graph Slepians is incorporated in a MI-decoding scheme, in which the informed projections are fed to a support vector machine (SVM) that casts a prediction regarding the type of intended movement. The employed MI-decoder is evaluated based on two publicly available datasets and its superiority against popular alternatives in the field is established. Computational efficiency is listed among its main advantages, since it involves only simple matrix operations, allowing to consider its use in real-time implementations.**

***Index Terms*— Graph signal processing (GSP), BCI, motor imagery, EEG.**

Manuscript received July 16, 2020; revised October 9, 2020; accepted December 21, 2020. Date of publication January 8, 2021; date of current version March 2, 2021. This work was supported in part by the Project MAMEM funding from the EU's H2020 Research and Innovation Program under Grant 644780 and in part by the Project NeuroMkt that has been co-financed by the European Regional Development Fund of the European Union and Greek National Funds through the Operational Program Competitiveness, Entrepreneurship, and Innovation, under the call RESEARCH–CREATE–INNOVATE under Project T2EDK-03661. *(Corresponding author: Kostas Georgiadis.)*

Kostas Georgiadis is with the AIIA Lab, Department of Informatics, Aristotle University of Thessaloniki, 54124 Thessaloniki, Greece, and also with the MKLab, Centre for Research and Technology Hellas, Information Technologies Institute, 57001 Thermi-Thessaloniki, Greece (e-mail: georgiaki@csd.auth.gr).

Dimitrios A. Adamos is with the Department of Computing, Faculty of Engineering, Imperial College London, London SW7 2BU, U.K., also with the NeuroInformatics.GRoup, 54124 Thessaloniki, Greece, and also with the Faculty of Fine Arts, School of Music Studies, Aristotle University of Thessaloniki (AUTH), 54124 Thessaloniki, Greece.

Spiros Nikolopoulos and Ioannis Kompatsiaris are with the MKLab, Centre for Research and Technology Hellas, Information Technologies Institute, 57001 Thermi-Thessaloniki, Greece.

Nikos Laskaris is with the AIIA Lab, Department of Informatics, Aristotle University of Thessaloniki, 54124 Thessaloniki, Greece, and also with the NeuroInformatics.GRoup, Aristotle University of Thessaloniki, 54124 Thessaloniki, Greece.

Digital Object Identifier 10.1109/TNSRE.2021.3049998

I. Introduction

BRAIN computer interfaces (BCIs) provide alternative communication (or control) pathways between the human brain and an external device [1], [2], by decoding brain activity and "translating" it into machine commands without requiring any physical interaction. In the past decade, BCIs due to their design, have been successfully adopted as rehabilitation and communication tools for people with partial or complete loss of their motor functions [3]. Recently, BCIs have been also employed in non-medical settings such as gaming [4], virtual reality [5] and mental workload monitoring [6]. There are several means for realizing a BCI, with Electroencephalography (EEG) being the most prominent choice due to its noninvasiveness (i.e. brain activity is registered via sensors placed over the scalp), relatively low-cost, portability and good temporal resolution.

Endogenous BCIs, receive continuous attention within the BCI community as they can be harnessed by a user via mental commands without requiring external stimulation. This leads to self-initiated (i.e. self-paced) implementations, opposed to exogenous BCIs that are dependent to external triggers (e.g. visual stimulation [7], [8]), aiding thus in the communication restoration [9], the motor rehabilitation process [10] and the wheelchair/exoskeleton control [11]. Mental commands include among others, mental arithmetic [12], [13], (internal) speech imagination [14], [15], writing imagination [16] and movement imagination (or motor imagery (MI)) [17]–[19], with the latter being identified as the most prominent choice.

MI-BCIs are built upon the sensory motor rhythm (SMR), an activity identified when a movement is either planned or executed within the sensorimotor area. Early studies established the pattern of event-related desynchronization/synchronization (ERD/ERS), with a power decrease in μ band preceding the imagery movement [20] and a power increase in β band (also referred as beta-rebound) marking its completion [21]. Next, spatial filtering techniques were introduced as a means to decode the MI-activity, with common spatial filters (CSPs) being the most popular one [22]. The design of CSPs is based on the maximization of a variance ratio corresponding to two conditions to be contrasted (e.g. "left hand" vs. "right hand") and their popularity is a direct consequence of computational efficiency. In the following years, several variations/modifications of the original algorithm were proposed (e.g. [23]–[26]) that led to

more robust MI-decoding schemes. Very recently, MI-decoders exploiting non-temporal representation schemes have been introduced, including among others phase synchrony [27], complex networks [28] and Riemannian geometry [29], [30]. Finally, MI decoders, aligned with the contemporary trends in deep learning, have started to appear in the related literature (e.g. [31] and [32]).

GSP is an emerging field that provides signal analytic tools for signals registered over irregular domains (like the multichannel EEG recordings), via a unified framework that combines graph theory and signal processing notions [33]–[36]. The conjunction between GSP and brain signal analysis steps upon the fact that the human brain can be considered as a distributed and intricately networked complex system. GSP has been successfully adopted by the neuroscientific community, with the earliest approaches providing elegant brain decoding schemes build upon functional neuroimaging signals [37]–[39]. Recently, graph spectral representations have been employed for analyzing EEG data [40] and designing robust BCI decoders [41], [42]. Nevertheless, there are still several aspects of GSP that remain unexplored by the BCI research community and their successful incorporation in the field holds great promise.

It is the scope of this study to introduce a novel MI decoding scheme that is built upon the recently introduced technique of *Graph Slepian functions* [43], an informed graph spectral transform that can be tailored to provide emphasis on specific functional components of the brain network(s). By incorporating in the design of these functions, our discriminative learning algorithm for detecting the most informative sub-graph within the sensor array [44], we propose a novel data-driven technique that learns to associate EEG graph signals with mental commands. The introduced, principled and simultaneously intelligible, transform considers the coordinated brain activity as this captured over the cortex. It exploits the induced differences in covariation pattern between distinct MI conditions to construct spatial filters that facilitate the detection of activation traces, characteristic for the mental task(s) we would like to differentiate upon. This naturally leads to a brain decoding scheme that is implementable within the framework of an on-line BCI-system. Our MI decoder involves a linear support vector machine (SVM), has a personalized character and is realized via simple matrix operations. Its evaluation is carried out using two publicly available datasets with cued MI activations. The first dataset includes data from our experiments with motor-impaired and healthy individuals and is used to establish the decoder's efficiency. The second contains data from able-bodied participants and is used to verify the decoder's superiority against popular alternatives.

The remainder of this paper is organized as follows: Section II describes the methodology for formulating our MI decoder, Section III is dedicated to the obtained results and Section IV discusses the added value and limitations of the study and the future perspectives of this work.

II. Methods

A. Dataset Description and Validation Protocol

The proposed decoding scheme was evaluated using two publicly available datasets containing MI-related EEG data. The first dataset, denoted hereafter as ***MKLab***, was recently released by the authors of this study [45] and encompasses encephalographic activity registered during the participants' imaginary movement of either their left or right hand and can be accessed via Figshare.[1] A total of twenty two subjects, with no prior experience with MI-based BCIs, participated in the experiment, with eleven of them suffering from motor disabilities (6 of them with neuromuscular disease (NMD), denoted as N1, N2, ... N6, and five from Parkinson's disease (PD), denoted as P1, P2, ..., P5) and 11 able-bodied (coded as S1, S2, ..., S11) with their socio-demographic profiles being matched accordingly. As brain functions are affected differently by the two conditions, a fact that could have an impact on the decoder's performance, we have chosen to examine the subjects separately in two groups: the NMD group (7 males, aged 36.08 $\pm$ 6.45) consisting of subjects N1, N2, ... N6 and S1, S2, ..., S6 and the PD group (9 males, aged 57.90 $\pm$ 10.18), consisting of the remaining subjects. Participants were requested to perform either a left or right hand imagery movement for five seconds based on an arrow that appeared on the screen and dictated the type of the MI task. Subjects performed 40 MI trials in total, equally distributed among the two classes. Moreover, prior to the experiment initiation, a resting state condition was recorded for all subjects. The EEG recordings were made using the BePlusLTM Bioelectric Signal Amplifier,[2] with the encephalographic activity being captured by 61 sensors placed according to the 10-20 International System (see Fig. 1a) with a sampling frequency of 256Hz. A series of pre-processing steps were followed prior to the implementation of the decoding scheme, namely bandpass filtering within 0.5-45 Hz, artifact removal, and bad sensor detection. The interested reader is referred to [27] for a detailed description of the aforementioned steps.

The second dataset was Dataset IVa of BCI competition III [46]. In the followings, it is denoted as ***Dataset IVa*** and contains the encephalographic activity during the imagery movement of the participant's hand or foot. It was selected as a means to further validate our approach in a more demanding scenario (i.e. to discriminate between ipsilateral 'hand' and 'foot' MI). Five subjects (coded as aa, al, av, aw, ay) participated in 140 "hand" and 140 "foot" trials, each lasting for 3.5 seconds, with the brain activity being captured via 118 sensors at a sampling frequency of 100Hz. The training/test split had been provided by the competition and was different for each participant, with the training set comprised of 168, 224, 84, 56 and 28 trials for subjects aa, al, av, aw, ay respectively and with the remaining of the trials serving as the test set.

[1] https://figshare.com/articles/dataset/MAMEM_Phase_I_Dataset_-_A_dataset_for_multimodal_human-computer_interaction_using_biosignals_and_eye_tracking_information/5231053

[2] www.ebneuro.biz/en/neurology/ebneuro/galileo-suite/be-plus-ltm

Due to the different nature of the datasets, two distinct validation protocols were employed. At first, in the case of the MKLab dataset, a leave-one-(trial)-out-cross-validation (LOOCV) scheme was used, mainly due to the limited amount of training data: a) each trial in turn was left out serving as a test set, b) the remainder of the trials were used for training the decoder, c) a label was predicted and compared with the "true class" of the trial. Secondly, in the case of Dataset IVa, the train-test set split had been defined by the competition organizers. As this partition was the most common choice among research groups, we opted for the same validation protocol aiming for fair comparisons.

B. Graph Fourier Transform (GFT)

GFT is one of the cornerstones of graph signal processing and blends the notion of classical Fourier transform with concepts from spectral graph theory. A graph signal is formally defined as a function that assigns real-valued vectors to the ordered set of nodes in a given graph ([33], [34]). In this context, GFT aims at analyzing the signals that reside on the graph and not the graph itself. According to graph theory, a weighted graph can be described as a triplet $G = \{V, E, \boldsymbol{W}\}$. $V = \{1, 2, \ldots, |V|\}$ denotes the node set. E denotes the edge-set, that indicates the existence (or not) of a connection between nodes. Finally, $\boldsymbol{W}$ is a $|V| \times |V|$ symmetric weighted adjacency matrix incorporating the quantification of pairwise inter-node relationships. The graph's connectivity pattern is encapsulated in the so-called *shift operator*, with the most popular choice being the graph Laplacian $\boldsymbol{L} = \boldsymbol{D} - \boldsymbol{W}$, with $\boldsymbol{D}$ denoting the degree matrix, a diagonal matrix with elements $d_{ii} = \sum_{j=1}^{|V|} w_{ij}$. The eigenanalysis of graph Laplacian, $\boldsymbol{L}$, results in a complete set of basis functions for analyzing the graph signals defined over G [33]. Based on the level of associated eigenvalues $\lambda_k, k = 0, \ldots, |V|-1$, the eigenvectors are sorted in ascending order and gathered in a $|V| \times |V|$ matrix $\boldsymbol{U} = [\boldsymbol{u_0}, \boldsymbol{u_1}, \ldots, \boldsymbol{u_{|v|-1}}]$ which plays an instrumental role in GFT. The interpretation of the Laplacian eigenvectors and the corresponding eigenvalues in the graph setting can be made analogously with the basis functions and frequencies in the temporal setting. The eigenvectors linked with low-valued eigenvalues are known to be smoother (i.e. they demonstrate slow variations between neighboring nodes) compared to the rest ones. The physical meaning of the transform can easily be conceived by considering each eigenvector as an eigenmode that might participate in the formation of a given graph signal $\boldsymbol{x} \in \mathbb{R}^{|V|}$. Hence, the spectral graph decomposition of $\boldsymbol{x}$ can be derived, simply, via matrix multiplication:

$$\tilde{\boldsymbol{x}} = U^T \boldsymbol{x} \tag{1}$$

C. Graph Slepians

Slepian functions were originally proposed in [43] as optimal solutions to the problem of faithfully representing an 1D signal that is concentrated, simultaneously, in time and spectral domain. In essence, Slepian functions are a generalization of the prolate spheroidal wave functions that ensure a trade-off between temporal and spectral energy concentrations. Slepian functions are derived, as linear combinations of a truncated Fourier basis, via the eigendecomposition of a concentration matrix that appears in an objective function and has the form of a Rayleigh quotient.

Graph Slepians have been recently launched as functions that generalize the standard Slepians for graph signals [47], [48], by introducing the notions of *selectivity* and *bandwidth* that correspond to the imposed constrains. The former refers to the original graph domain, while the latter to the graph spectral domain. *Selectivity* controls the selection of a subset of nodes $B \subseteq V$ that demonstrate energy concentration at a maximum level and is encoded in the diagonal matrix $\boldsymbol{B} \in \mathbb{R}^{|V| \times |V|}$ with elements indicating the participation of a given node in a restricted subgraph of interest, i.e.:

$$b_{i,i} = \begin{cases} 1, & include \\ 0, & exlude \end{cases} \tag{2}$$

Bandwidth, on the other hand, is employed to impose the constraints in the spectral domain by retaining only low-frequency basis vectors (i.e. the eigenvectors associated with the N smallest eigenvalues) and forming a trimmed version of $\boldsymbol{U}$ denoted as $\bar{\boldsymbol{U}} \in \mathbb{R}^{|V| \times N}$. Both types of constraints are embodied in the *concentration matrix* $\boldsymbol{C} = \bar{\boldsymbol{U}}^T \boldsymbol{B} \bar{\boldsymbol{U}}$ and the problem of optimally localizing a graph signal $\boldsymbol{x} \in \mathbb{R}^{|V|}$ in both domains is transformed to maximizing the Rayleigh quotient:

$$r = \frac{\tilde{\boldsymbol{x}}^T \boldsymbol{C} \tilde{\boldsymbol{x}}}{\tilde{\boldsymbol{x}}^T \tilde{\boldsymbol{x}}} \tag{3}$$

Solving this problem boils down to the eigendecomposition of the concentration matrix and leads to the derivation of N eigenvectors $\{\tilde{\boldsymbol{s}}_k\}$, $k = 0, 1, \ldots, N-1$. Solution $\tilde{\boldsymbol{s}}_0$ is the one demonstrating the highest level of concentration (considering that eigenvalues have been arranged in increasing order). The matrix $\boldsymbol{S} \in \mathbb{R}^{|V| \times N}$ that contains the Slepian functions $\boldsymbol{s_k}$, as graph-signals, in its column can be easily deduced using the matrix $\tilde{\boldsymbol{S}}$ which is formed by collecting $\{\tilde{\boldsymbol{s}}_k\}$:

$$\boldsymbol{S} = \bar{\boldsymbol{U}} \tilde{\boldsymbol{S}} \tag{4}$$

The Slepian vectors are orthonormal over the overall graph and orthogonal over the constrained subgraph associated with $\boldsymbol{B}$.

D. Graph Slepians for EEG Activity From Cortical Networks

Brain network(s) usually conform with the connectivity patterns estimated within and between brain regions and their function can therefore be described via signals over the corresponding graphs. In the case of an electroencephalographically observed cortical network, and using the mathematical notations previously introduced, the most common approach is to assign the recording sites (or sensor array) as the nodes of a graph G and form $\boldsymbol{W}$ by tabulating the connectivity strengths between the various sensor pairs. In this work, $\boldsymbol{W}$ is formulated based on the sensors' spatial arrangement in the 2D space, with each non-diagonal entry being defined as $w_{i,j} = \exp(-\frac{d(\boldsymbol{c_i}, \boldsymbol{c_j})}{\rho})$, where $d(\boldsymbol{c_i}, \boldsymbol{c_j})$ is the Euclidean distance between the 2D Cartesian coordinate

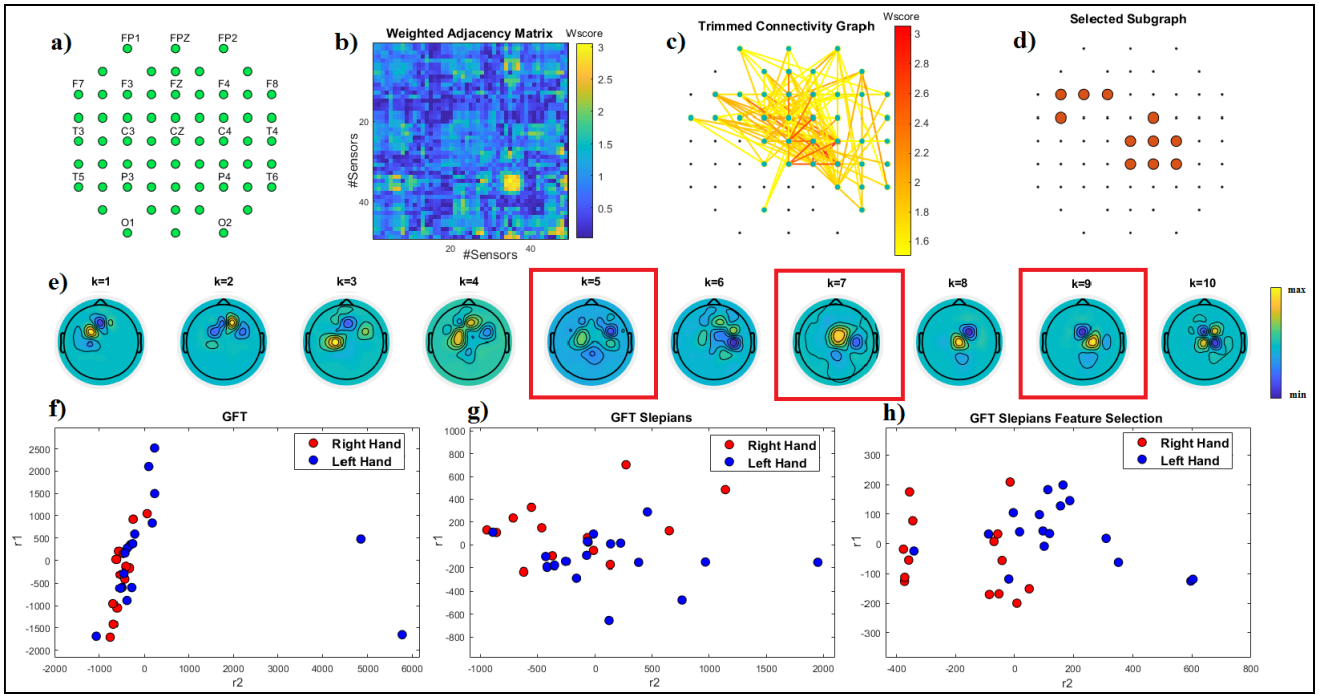

Fig. 1. The design of Graph Slepians exemplified for P1 subject. a) Topographical representation of EEG sensor array in a 2D space. b) The Weighted Adjacency matrix derived in discriminative manner based on the spatial covariance matrices (i.e. $W_{Contrast}$) of the training trials: each (i,j) entry reflects the Wilcoxon score corresponding to the contrast between the two MI-tasks c) The associated connectivity graph, drawn over the sensor-array, after a simple sparsification step (only edges with Wscore>1.5 have been retained). d) The sensors selected via the DS-algorithm that constitute the subgraph B. e) The Graph Slepian functions, ordered by increasing eigenvalue, presented as graph signals with the signals enclosed in red boxes being the selected ones (S_{sel}). f) MDS representation of an instantiation of the training trials based on the *classical* GFT. g) The corresponding MDS map when all ten Graph Slepians are employed. h) The corresponding MDS map when the most discriminative Graph Slepians are employed.

vectors of the two sensors i and j and ρ is the average inter-sensor distance. On the contrary, all diagonal elements $w_{i,i}$ are set to zero to avoid self-loops. Equipped with this formulation, eq(1) is updated to implement efficiently the GFT along the temporal dimension of a multichannel EEG signal $\boldsymbol{X} = [\boldsymbol{x_1}, \boldsymbol{x_2}, \ldots, \boldsymbol{x_T}] \in \mathbb{R}^{|V| \times T}$, where T denotes the number of samples in time, as follows:

$$\tilde{\boldsymbol{X}} = \boldsymbol{U}^T \boldsymbol{X} \tag{5}$$

The meaning of the previous equation is that the GFT of a temporal sequence of graph signals (or instantaneous electric fields) can be applied via a matrix operation. The resulting projections reflect the (modulated in time) matching of multichannel signal with the eigenmodes of the topological graph G.

In the above GFT analysis, all nodes and eigenmodes are treated equivalently and this might hinder the use of anatomical information (like which sensor are close to the neural sources of a signal of interest). We believe that the graph Slepians constitute an invaluable strategy for inducing such extra information in GFT and proceed with the introduction of a data-driven methodology to design them, on a personalized level, based on the available training set of labeled trials. Starting with *selectivity*, the delineation of a subgraph B of interest, in which the spectral analysis will put emphasis on, is performed using a graph-clustering algorithm in the way that it was recently introduced for sensor-selection in covariance-based decoding of MI [44]. The particular algorithm, known as Dominant-Set (DS) algorithm [49], [50], identifies the most coherent group of nodes in a given connectivity graph. The Appendix provides a short description of its adaptation towards discriminative learning in the setting of multichannel EEG signals. In a nutshell, by statistically contrasting, based on trials included in the training set, the two recording conditions (e.g. 'left' vs. 'right'), we obtain a ($|V| \times |V|$) weighted adjacency matrix $\boldsymbol{W_{contrast}}$, in which two sensors are strongly connected if their signals appear to covary differently across conditions. This matrix is then fed to the DS algorithm that leads to a vector $\mathbf{z}^*$ of binary values corresponding to the participation indices of eq(2). In other words, the DS-algorithm articulates the *selectivity* specifications for our Graph Slepians. On the other hand, the *bandwidth* corresponds to the selection of the number $N \leq |V|$ of GFT basis vectors, with the lowest frequencies and its precise extend parameters that may be selected experimentally. The upper part of Fig.1 exemplifies the design of Graph Slepians based on data from subject P1, with Fig.1b illustrating $\boldsymbol{W_{contrast}}$ and Fig.1c providing its sparsified version (that facilitates a less-cluttered visualization). The sensors elected (by the DS algorithm) to participate in the subgraph B are highlighted with a light brown color in Fig.1d.

Once *selectivity* and *bandwidth* have been defined, the set of Graph Slepians can be readily derived via eigenanalysis of the concentration matrix $\boldsymbol{C}$ and eq(4). Returning to the previous example, the 10 eigenvectors corresponding to the first 10 smallest eigenvalues (i.e. $N = 10$) are presented on

Fig. 1e. Following the convention of eq(5), the projection of the multichannel signal in the domain of Graph Slepians takes the form:

$$\hat{\boldsymbol{X}} = \boldsymbol{S}^T \boldsymbol{X} \tag{6}$$

E. Feature Extraction and Selection

The derived by eq.(6) matrix $\hat{\boldsymbol{X}} \in \mathbb{R}^{N\times T}$ contains the time-indexed projections of the multichannel EEG signal in the graph Slepian domain and reflects the time-varying contribution of the corresponding eigenmodes. In this regard, an efficient feature extractor can be implemented via the time-integrated power of each eigenmode:

$$\boldsymbol{p}\,(m) = \frac{1}{T}\sum_{t=1}^{T}\left|\hat{X}(m,t)\right|^2, \quad m = 1, 2, \ldots, N \tag{7}$$

In this way, each trial is described by a N-dimensional power profile $\boldsymbol{p} \in \mathbb{R}^N$, that plays the role of a feature vector and represents the distribution of signal-power within the graph Slepian domain. The feature extraction step is then followed by a feature selection step. The design, implied in the latter step, is carried out based on the training set of trials. However, the selection applies to the test set as well. With the scope of maximally differentiating between the two MI-conditions, the single-trial power profiles (along with the associated class labels), are fed to a feature-ranking algorithm to measure the potential of each Graph Slepian in the subsequent classification. Without loss of generality, Matlab's *rankfeatures* command (Matlab 2019a; with the particular option for Wilcoxon statistical score, denoted here as W_{score}) is implied in the rest of this paper. Each Graph Slepian function (or spatial filter) is associated with a score that quantifies its discriminatory power. The eigenmodes are ranked in descending order, with the first ones being expected to lead in more competent classifiers. To finalize this *filter-approach* to feature selection, a random permutation technique is employed as a means of identifying the exact number of components to be selected [51]. More specifically, rankfeatures scores are estimated several times, upon random re-labeling, resulting to a distribution of W_{score} values that corresponds to the "null-hypothesis" of no class separation. The 95% percentile limit of the aforementioned scores is utilized as the threshold. The eigenmodes with scores higher than the identified threshold are the selected ones and are tabulated in $S_{sel} \in \mathbb{R}^{|V|\times A}$, with A denoting the number of the selected spatial filters. It is interesting to notice that the above feature selection step complies with the standard notion of "graph signal filtering" [35], where only some spectral modes are kept during the reconstruction of the graph signal. The three selected eigenmodes (i.e. A = 3, with $k = 9, 7$ and 5, sorted in descending order) for the previously introduced example are enclosed in a red box in Fig.1e. The impact that this step has on class separability is easily justified by visually inspecting and comparing the multidimensional scaling (MDS) representations, shown in Fig.1f-h, for the previous example. In the bottom line of Fig.1 shown are the (low-dimensional representation of) power profiles obtained from the *classical* GFT, the "full" set Graph Slepians and the selected Graph Slepians transform.

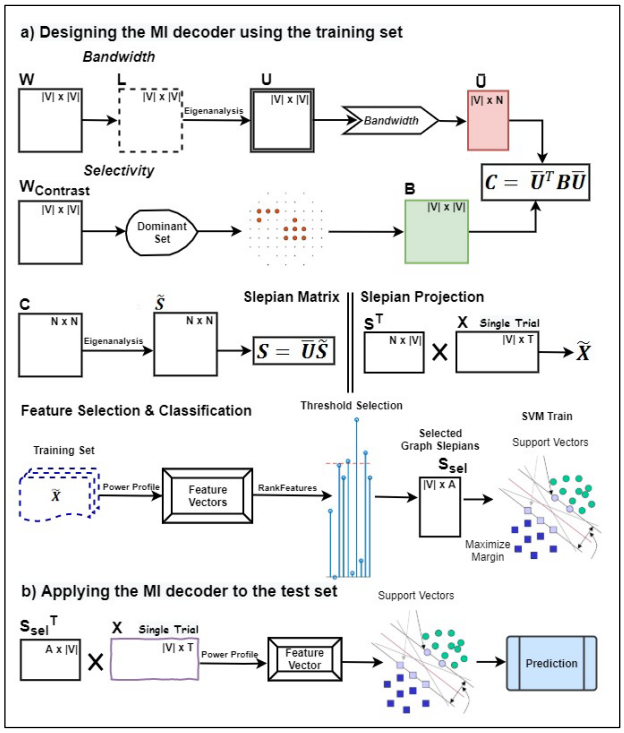

Fig. 2. Flowchart of the proposed methodology.

F. Graph Slepians (GSLs) Based MI-Decoder: Classification and Performance Evaluation

To fully justify the introduced technique for tailoring GSLs, we have incorporated it in an MI-decoder that utilizes a linear SVM that acts on the associated power profiles (see Fig.2). SVMs are well-established classification tools within the BCI community, as they provide robust solutions for a wide variety of EEG-related problems [52], including SMR-related ones [53]. Considering a binary classification scenario, the training stage incorporates the identification of the optimal hyperplane that guarantees optimal separability among the two classes by maximizing the margin between them. The selected hyperplane is the one that is expected to cope better with unseen (i.e. test) data, while the class of unseen data is determined by the "side" of the hyperplane in which the data sample lies. For the purposes of this study, the linear hyperplane is selected due to its low computational cost and its rigorous predictions, features of paramount importance for any online BCI implementation. Consequently, classification accuracies, are used to evaluate the performance of the proposed decoder, tailored to each cross-validation scheme and independently estimated for each subject. The application of the MI-decoder to a test trial merely consists of a simple matrix multiplication and the generation of its power profile (as illustrated in Fig. 2b), with its complexity (C_{GSL}) being formulated as $C_{GSL} = O\,(A\,|V|\,T) + O\,(A) = O\,(A\,|V|\,T)$. Considering that i) $A \ll N$, ii) |V| is 256 in the most dense sensor array, and iii) T depends

on the duration of the performed task (typically not exceeding the interval of 4 seconds), the computational efficiency of the proposed decoder can be justified. The flowchart of the proposed decoding scheme is provided in Fig. 2 and is exemplified in a Matlab-based demonstration being available online.[3] More specifically, the top panel of Fig.2 presents the designing-stage for the proposed decoder. Given a set of MI trials of known labels (i.e. the training set) the decoder's initial steps require the formulation of bandwidth and selectivity, with the former being a trimmed version of the eigenvectors derived by the eigendecomposition of $\mathbf{W}$ and the latter indicating the sensors that demonstrate high energy concentration levels identified by the DS algorithm. The eigendecomposition of the concentration matrix will then lead to the Slepian matrix ($\mathbf{S}$) that includes the Slepian functions as shown in eq.(4). The projection of each training trial into the Graph Slepian domain consists of a simple multiplication between the trial and $\mathbf{S}$ (see eq.(6)). The most discriminative power profiles are then used for training a linear SVM. On the other hand, the bottom panel of Fig.2 illustrates the application of the decoder to an unlabeled MI trial, that is realized via multiplication with the selected Graph Slepians, generation of the power profile and SVM prediction.

III. Results

A. GSL-Decoder in MKLab Dataset

Working in a personalized fashion all trials were first band-pass filtered within the frequency range of 8-25 Hz, $\mathbf{W}$ was formulated using the Euclidean distance of the sensors' 2D coordinates,[4] while the 4-second post-stimulus brain activity was selected for the projection in the Graph Slepian domain. *Selectivity* constraints were identified (via the DS algorithm) separately in each iteration of the LOOCV protocol, while the *bandwidth* was set to N=10 for all subjects. This choice was defined after an initial experimentation during which the performance of the decoder had been monitored for variable N (see later in this section). An example of GSLs design has been provided in Fig.1, where it can be noticed that the subgraph of interest consists, mainly, of sensors lying over the sensorimotor area, an attribute that can be characterized as neurophysiologically meaningful considering that the specific area is highly activated when the particular mental task is performed. Additionally, the GSL vectors, derived from eq.(4), can be seen in Fig.1e, with the selected ones being enclosed in red boxes. These graph signals reflect, as well, high(er) levels of activity in the sensory motor area compared to the remaining GSLs, aiding thus in the discrimination between the two MI tasks.

A linear SVM (with the regularization parameter c set to 1) was used to cast the prediction for each iteration of the LOOCV scheme, using only the selected Graph Slepians. By averaging across trials the number of correct predictions, the classification scores shown in Table I and Table II, were derived.

[3]Matlab Code: https://neuroinformatics.gr/downloads/Covariation_Informed_Graph_Slepians_for_Motor_Imagery_Decoding.zip

[4]The 2D coordinates are included in the provided Matlab code.

TABLE I
CLASSIFICATION PERFORMANCE (%) IN THE "LEFT VS RIGHT" TASK FOR THE NEUROMUSCULAR (NMD) GROUP IN MKLAB DATASET

	GSL	GFT	CSP		GSL	GFT	CSP
Sub. ID	**Acc.** (#nodes)	**Acc.**	**Acc.**	**Sub. ID**	**Acc.** (#nodes)	**Acc.**	**Acc.**
S1	**90.32** (10)	61.29	58.06	N1	**94.44** (6)	66.67	52.78
S2	**93.54** (7)	64.51	54.84	N2	**96.87** (7)	56.25	68.75
S3	**87.09** (9)	53.33	56.67	N3	**93.54** (8)	64.52	54.84
S4	**94.59** (7)	54.05	59.46	N4	**91.67** (9)	55.56	58.33
S5	**93.75** (8)	59.37	53.13	N5	**96.77** (7)	70.97	61.29
S6	**93.93** (7)	54.55	51.52	N6	**96.77** (8)	58.06	61.29
avg	**92.20** (8)	57.85	55.61	avg	**95.01** (7.5)	62.00	59.54

TABLE II
CLASSIFICATION PERFORMANCE (%) IN THE "LEFT VS RIGHT" TASK FOR THE PARKINSONIAN (PD) GROUP IN MKLAB DATASET

	GSL	GFT	CSP		GSL	GFT	CSP
Sub. ID	**Acc.** (#nodes)	**Acc.**	**Acc.**	**Sub. ID**	**Acc.** (#nodes)	**Acc.**	**Acc.**
S7	**84.38** (9)	78.13	62.50	P1	**93.54** (6)	70.97	64.51
S8	**76.47** (8)	58.82	52.94	P2	**76.66** (7)	60.00	53.33
S9	**74.19** (6)	64.51	58.06	P3	**78.12** (5)	65.63	59.37
S10	**71.42** (7)	60.00	57.14	P4	**79.31** (7)	58.62	55.14
S11	**75.86** (6)	58.62	51.72	P5	**87.87** (8)	63.63	60.60
avg	**76.46** (7.2)	64.01	56.47	avg	**83.10** (6.6)	63.77	58.59

For comparison purposes, the classification scores from two additional MI-decoders have also been tabulated. The former was built over standard GFT and the latter over CSP representation. In the first case, the eigenmodes of the "topographical" Laplacian $\boldsymbol{L}$ were used, while in the second case 3 pairs of spatial filters (associated with the three largest and smallest eigenvectors as proposed in [23]) were employed in the feature extraction step, while the feature-selection and classification procedures were identical to the ones used in the case of our decoder (see Fig.2).

Table I tabulates the classification scores for the NMD group, while Table II the scores for the PD group. It is evident that the proposed decoding scheme (GSL) outperforms the GFT-based and CSP-based decoders, on a subject basis and on average performance as well, and this trend is consistent for both groups (i.e. NMD and PD).

By examining each table independently and starting with Table I, it is noticeable that when the GSL decoder is employed, the classification scores are high for all subjects (except for subject S3) demonstrating classification scores higher than 90%. In total, the performance level exceeds

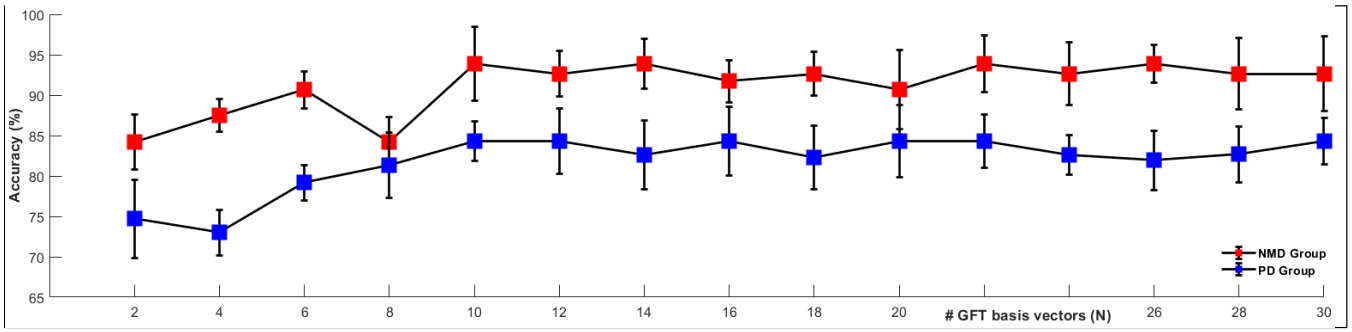

Fig. 3. The dependence of GSL-decoder's performance on the bandwidth, in the case of MKLab dataset.

93% in terms of Accuracy. Moreover, it is important to stress out here that the process of imposing the *selectivity* constrains results in the selection of eight nodes on average with the majority of them lying over the sensory motor area as previously discussed. This proves both the decoder's effectiveness and its low computational cost, constituting the implementation ideal for any online BCI paradigm.

The proposed decoder's superiority against GFT is also established here, with the average improvement reaching 30% and the subject specific analysis providing similar findings as well. The comparison between CSP and the GSL-decoder also favors the latter, with the average improvement exceeding 30%. Another noticeable fact here is the slightly higher classification scores obtained for motor impaired participants compared to the age matched healthy group regardless of the employed decoding mechanism; a trend that can be attributed to the disease's gradual progression as discussed in [27].

Similar conclusions are drawn from the analysis of Table II. The comparison of the introduced GSL decoder against the two alternatives indicates relative difference in performance that is higher than 20%. In this group, the average number of nodes included in the subgraph of interest (regarding the *selectivity* criterion) is seven and once again the included nodes arise within the sensorimotor area (e.g. the selected subgraph for subject P1).

To provide some evidence about the relative insensitivity of the decoder's performance to the actual number N (*bandwidth* parameter), we first estimated the subject-specific profiles corresponding to the classification accuracy as a function of the number of selected GFT-eigenmodes, and then averaged across subjects. Fig. 3 includes the averaged profile derived for both the NMD and the PD group, making clear the value of $N = 10$ was a reasonable choice considering also the computational load accompanying the larger bandwidths. It is worth mentioning here that no difference was observed, regarding the number of selected eigenmodes, between the able bodied and the motor impaired participants.

B. GSL-Decoder in Dataset IVa

Working in a similar fashion, i.e. towards personalized design of the decoder, all trials were first filtered in the 8-30Hz (as done in previous published works with the same data), $\mathbf{W}$ was derived upon the Euclidean distance of the sensors' 2D coordinates[5] and the projections to the graph Slepian domain were made upon a 2-second interval (initiated 0.5 seconds after the onset). In this case *selectivity* constrain and graph filtering were implemented only once (since the train-test split was provided), while *bandwidth* was experimentally set to 50. The classifier's training process was also carried once, with the SVM (linear kernel; c equals to 1) casting the predictions for all test trials and with the averaged correctly recognized trials marking the classification accuracy.

TABLE III
CLASSIFICATION PERFORMANCE (%) IN THE "HAND VS FOOT" TASK FOR DATASET IVA

	GSL	**GFT**	**CSP**	**TR CSP**	**WTR CSP**	***l1* -CSP**
Sub. ID	***Acc.*** (#nodes)	***Acc.***	***Acc.***	***Acc.***	***Acc.***	***Acc.***
aa	**85.71** (13)	74.11	66.07	71.43	69.64	78.56
al	**98.21** (10)	**98.21**	96.43	96.43	**98.21**	**98.21**
av	**75.00** (15)	69.90	47.45	63.27	54.59	54.08
aw	**85.27** (18)	76.79	71.88	71.88	71.88	80.35
ay	**90.48** (19)	76.98	49.60	86.90	86.90	83.33
avg	**86.93** (15)	79.19	66.29	77.98	76.24	78.91

Table III tabulates the classification accuracy when the proposed decoder is employed and also provides a direct comparison with the GFT approach, the CSP algorithm and three of its popular alternatives (namely TRCSP [23], WTRCSP [23] and 11-CSP [24]). GSL-based decoder outperforms the rest ones, with the most noticeable difference concerning subjects aa and ay.

C. GSL-Decoder in Resting State Vs MI Task (MKLab Dataset)

The final part of our analysis includes the design and application of the GSL-decoder in a different, but very important, classification task. This of discriminating segments of resting state from trials of MI-activity (independently of movement

[5]The sensors' 2D coordinate vectors are incorporated in the provided dataset.

TABLE IV
CLASSIFICATION PERFORMANCE (%) IN THE "REST VS MI" TRIAL FOR MKLAB DATASET

Sub. ID	Acc.	Sub. ID	Acc.	Sub. ID	Acc.	Sub. ID	Acc.
S1	97.50	N1	100.00	S7	100.00	P1	100.00
S2	100.00	N2	100.00	S8	95.00	P2	97.50
S3	96.67	N3	97.50	S9	100.00	P3	100.00
S4	100.00	N4	97.22	S10	100.00	P4	95.00
S5	96.88	N5	100.00	S11	92.50	P5	100.00
S6	92.50	N6	96.77				98.50
avg	97.26	avg	98.58	avg	97.50	avg	98.50

direction). This task can be associated (up to a certain extend) with the simulation of a self-paced BCI, where a "switch" controlled by the user will ignite the subsequent MI-decoder. The resting state recordings (following the preprocessing pipeline as described in section II.A) were segmented into 20 resting-state trials. Next, 20 MI trials equally distributed among the two classes ("left" and "right") were randomly selected to form an equally sized dataset consisting of MI trials of both conditions. Following the (same) series of steps required to build the MI decoder, an "SVM-switch" for identifying the initiation (or not) of an MI task regardless of its class label (i.e. of both directions) was crafted.

The classification accuracy was again derived based on the LOOCV protocol, but this time its measurement was repeated multiple times with different instantiations of the MI trials dataset. The classification accuracy (across bootstraps) was opted as the evaluation mechanism of the detection decoder with the obtained results being tabulated in Table IV. The near optimal performance of the decoder for almost all subjects indicates its suitability for reliably detecting the triggered SMR related activity.

IV. DISCUSSION

Graph theory concepts have been widely employed by the network neuroscience community to characterize brain function [54]. For a coarse, EEG-guided, reconstruction of brain network(s), it is common practice to treat the recording sites as graph nodes and exploit the sensor topographical arrangement for building the corresponding weighted adjacency matrix. The emerging rise of interest in GSP theory can be attributed to the fact that its fundamental concepts (e.g. GFT, graph filtering) are generalizations of the ones employed in the standard domains (of either time or space) and can therefore be interpreted analogously.

In this work, a novel MI-decoding scheme is introduced, based on the concept of *Graph Slepian functions,* that emphasizes specific graph and spectral graph components. The graph domain constraints are imposed by the graph clustering DS algorithm (see Fig. 1d). They provide the discriminative learning character in our decoder and involve personalization. On the other hand, the constraints imposed in spectral graph domain take the form of a low-pass filtering that is implemented by disregarding the fast GFT eigenmodes. The validation of the decoder was performed based on two publicly available datasets (i.e. MKLab dataset and Dataset IVa of BCI competition III) and revealed its superiority relatively to popular alternatives in the field and, also, the standard GFT (see Table I-Table III). It is important to mention here that the success of GSLs in the discrimination between two mental tasks does not concern only able-bodied participants but also people suffering from motor disabilities (i.e. NMD and PD) who are the main target group of users for the BCI systems.

Apart from the documented effectiveness of the decoder, in terms of classification accuracy, its computational efficiency and feasibility of incorporation in an online BCI-system should be underlined. The decoder relies on simple signal analytic operations that guarantee low computational cost and swift responses (refer to Fig. 2). In addition, the incorporation of the DS algorithm in GSL-design ensures the exclusion of bad or artifact contaminated sensors and therefore enhances the decoder's robustness while also lifts the necessity of using online denoising algorithms.

At this point, the limitations of this study and some issues that were left untreated should be considered, starting with the possibility of an online implementation of the decoder, in which the decoder could be "self-initiated" by the user (and not externally triggered as in the case of the experimental data). The transition to an online scenario appears feasible, due to the decoder's ability to provide near real-time response. Furthermore, its verified ability to reliably discriminate between resting-state and MI-segments (as shown in section III.C) enables us to envision a self-paced decoding scheme that proceeds in two stages (as presented in our previous study [41]). The first stage will include a "GSL-based switch" with the decoder detecting an MI-event (as deviation from an "idle" brain state), while the second stage will include a "GSL-based discriminator" with the decoder identifying the type of the MI-event (i.e. its direction). Finally, since BCIs should aim at serving multiple classes so as to provide higher degrees of freedom to their users, the transition of our decoder towards multiclass implementation remains to be explored in future extensions of this work, with one option being the adaptation of a one vs all strategy.

APPENDIX

Given a weighted adjacency matrix that contains the pairwise affinity relationships in a graph, the dominant-set (DS) algorithm seeks the subset of nodes demonstrating the highest cohesiveness levels.

Here, the weighted adjacency matrix, denoted as $\boldsymbol{W}_{\boldsymbol{contrast}} \in \mathbb{R}^{|V|\times|V|}$, is formulated so as to indicate the differences in the spatial covariance structure between the two MI-tasks, as estimated upon the training set. More specifically, firstly the sample covariance matrix (SCM) of each single trial $\boldsymbol{X}_l \in \mathbb{R}^{|V|\times T}$ is estimated as $\boldsymbol{C}_l = \boldsymbol{X}_l \boldsymbol{X}_l^T/(T-1) \in \mathbb{R}^{|V|\times|V|}$ and treated as the trial-specific feature vector. Then, the vectorized versions of the derived SCMs for the entirety of the training set (accompanied by their corresponding labels) are fed to a feature ranking algorithm that determines the separability among the two classes by using as evaluation criterion the statistical index of Wilcoxon test. Finally, the obtained scores (that refer to each pairwise covariation independently) are

reshaped in the form of a |V| × |V| matrix, providing the $\boldsymbol{W_{contrast}}$.

Returning to the Dominant-Set algorithm, the problem of identifying the most cohesive subgraph, given $\boldsymbol{W_{contrast}}$, can be solved using the approach of replicator dynamics [49] by identifying the vector $\boldsymbol{z}$ that maximizes the objective function of cohesiveness:

$$F(z) = \boldsymbol{z}^{\boldsymbol{T}} \boldsymbol{W_{contrast}} \boldsymbol{z} \tag{A.1}$$

subject to $\boldsymbol{z} \in \Delta$, where $\Delta = \{\boldsymbol{z} \in \mathbb{R}^{|V|} : z_i \geq 0, \forall i \; and \; \sum_{i=1}^{|V|} z_i = 1\}$. The algorithm converges in a swift fashion to a vector $\boldsymbol{z}^*$ [50] that indicates the dominant group of nodes and actually defines the selectivity matrix $\boldsymbol{B}$, with the "included" nodes being the ones identified by the DS algorithm, with eq.(2) being updated accordingly:

$$b_{i,i} = \begin{cases} 1, & if \; z_i^* \geq 0 \\ 0, & otherwise \end{cases} \tag{A.2}$$

REFERENCES

[1] M. A. Lebedev and M. A. L. Nicolelis, "Brain-machine interfaces: From basic science to neuroprostheses and neurorehabilitation," *Physiol. Rev.*, vol. 97, no. 2, pp. 767–837, Apr. 2017.

[2] C. S. Nam, A. Nijholt, and F. Lotte, *Brain-Computer Interfaces Handbook: Technological and Theoretical Advances*. Boca Raton, FL, USA: CRC Press, 2018.

[3] S. Moghimi, A. Kushki, A. M. Guerguerian, and T. Chau, "A review of EEG-based brain-computer interfaces as access pathways for individuals with severe disabilities," *Assistive Technol.*, vol. 25, no. 2, pp. 99–110, Apr. 2013.

[4] H. Gurkok, A. Nijholt, and M. Poel, "Brain-computer interface games: Towards a framework," in *Handbook of Digital Games and Entertainment Technologies*. Singapore: Springer, 2017, pp. 133–150.

[5] F. Lotte *et al.*, "Combining BCI with virtual reality: Towards new applications and improved BCI," in *Towards Practical Brain-Computer Interfaces*. Berlin, Germany: Springer, 2012, pp. 197–220.

[6] M. V. Kosti, K. Georgiadis, D. A. Adamos, N. Laskaris, D. Spinellis, and L. Angelis, "Towards an affordable brain computer interface for the assessment of programmers' mental workload," *Int. J. Hum.-Comput. Stud.*, vol. 115, pp. 52–66, Jul. 2018.

[7] H. Riechmann, A. Finke, and H. Ritter, "Using a cVEP-based brain-computer interface to control a virtual agent," *IEEE Trans. Neural Syst. Rehabil. Eng.*, vol. 24, no. 6, pp. 692–699, Jun. 2016.

[8] K. Georgiadis, N. Laskaris, S. Nikolopoulos, and I. Kompatsiaris, "Discriminative codewaves: A symbolic dynamics approach to SSVEP recognition for asynchronous BCI," *J. Neural Eng.*, vol. 15, no. 2, Apr. 2018, Art. no. 026008.

[9] C. Guger *et al.*, "Complete locked-in and locked-in patients: Command following assessment and communication with vibro-tactile P300 and motor imagery brain-computer interface tools," *Frontiers Neurosci.*, vol. 11, p. 251, May 2017.

[10] A. A. Frolov *et al.*, "Post-stroke rehabilitation training with a motor-imagery-based brain-computer interface (BCI)-controlled hand exoskeleton: A randomized controlled multicenter trial," *Frontiers Neurosci.*, vol. 11, p. 400, Jul. 2017.

[11] K. Choi and A. Cichocki, "Control of a wheelchair by motor imagery in real time," in *Proc. Int. Conf. Intell. Data Eng. Automated Learn.* Berlin, Germany: Springer, 2008, pp. 330–337.

[12] Q. Wang and O. Sourina, "Real-time mental arithmetic task recognition from EEG signals," *IEEE Trans. Neural Syst. Rehabil. Eng.*, vol. 21, no. 2, pp. 225–232, Mar. 2013.

[13] S. Dimitriadis, Y. Sun, N. Laskaris, N. Thakor, and A. Bezerianos, "Revealing cross-frequency causal interactions during a mental arithmetic task through symbolic transfer entropy: A novel vector-quantization approach," *IEEE Trans. Neural Syst. Rehabil. Eng.*, vol. 24, no. 10, pp. 1017–1028, Oct. 2016.

[14] L. Wang, X. Zhang, X. Zhong, and Y. Zhang, "Analysis and classification of speech imagery EEG for BCI," *Biomed. Signal Process. Control*, vol. 8, no. 6, pp. 901–908, Nov. 2013.

[15] C. H. Nguyen, G. K. Karavas, and P. Artemiadis, "Inferring imagined speech using EEG signals: A new approach using Riemannian manifold features," *J. Neural Eng.*, vol. 15, no. 1, Feb. 2018, Art. no. 016002.

[16] Z. Qiu *et al.*, "Optimized motor imagery paradigm based on imagining Chinese characters writing movement," *IEEE Trans. Neural Syst. Rehabil. Eng.*, vol. 25, no. 7, pp. 1009–1017, Jul. 2017.

[17] D. J. McFarland and J. R. Wolpaw, "Sensorimotor rhythm-based brain–computer interface (BCI): Feature selection by regression improves performance," *IEEE Trans. Neural Syst. Rehabil. Eng.*, vol. 13, no. 3, pp. 372–379, Sep. 2005.

[18] T. Solis-Escalante, G. Müller-Putz, and G. Pfurtscheller, "Overt foot movement detection in one single Laplacian EEG derivation," *J. Neurosci. Methods*, vol. 175, no. 1, pp. 148–153, Oct. 2008.

[19] B. Xia *et al.*, "A binary motor imagery tasks based brain-computer interface for two-dimensional movement control," *J. Neural Eng.*, vol. 14, no. 6, Dec. 2017, Art. no. 066009.

[20] G. Pfurtscheller and F. H. L. da Silva, "Event-related EEG/MEG synchronization and desynchronization: Basic principles," *Clin. Neurophysiol.*, vol. 110, no. 11, pp. 1842–1857, Nov. 1999.

[21] E. Formaggio *et al.*, "Modulation of event-related desynchronization in robot-assisted hand performance: Brain oscillatory changes in active, passive and imagined movements," *J. Neuroeng. Rehabil.*, vol. 10, no. 1, p. 24, 2013.

[22] H. Ramoser, J. Muller-Gerking, and G. Pfurtscheller, "Optimal spatial filtering of single trial EEG during imagined hand movement," *IEEE Trans. Rehabil. Eng.*, vol. 8, no. 4, pp. 441–446, Dec. 2000.

[23] F. Lotte and C. Guan, "Regularizing common spatial patterns to improve BCI designs: Unified theory and new algorithms," *IEEE Trans. Biomed. Eng.*, vol. 58, no. 2, pp. 355–362, Feb. 2011.

[24] B. Wang *et al.*, "Common spatial pattern reformulated for regularizations in brain-computer interfaces," *IEEE Trans. Cybern.*, early access, Apr. 22, 2020, doi: 10.1109/TCYB.2020.2982901.

[25] A. Jiang, J. Shang, X. Liu, Y. Tang, H. K. Kwan, and Y. Zhu, "Efficient CSP algorithm with spatio-temporal filtering for motor imagery classification," *IEEE Trans. Neural Syst. Rehabil. Eng.*, vol. 28, no. 4, pp. 1006–1016, Apr. 2020.

[26] H. Wang *et al.*, "An approach of one-vs-rest filter bank common spatial pattern and spiking neural networks for multiple motor imagery decoding," *IEEE Access*, vol. 8, pp. 86850–86861, 2020.

[27] K. Georgiadis, N. Laskaris, S. Nikolopoulos, and I. Kompatsiaris, "Exploiting the heightened phase synchrony in patients with neuromuscular disease for the establishment of efficient motor imagery BCIs," *J. Neuroeng. Rehabil.*, vol. 15, no. 1, pp. 1–18, Oct. 2018.

[28] F. De Vico Fallani and D. S. Bassett, "Network neuroscience for optimizing brain–computer interfaces," *Phys. Life Rev.*, vol. 31, pp. 304–309, Dec. 2019.

[29] A. Barachant, S. Bonnet, M. Congedo, and C. Jutten, "Classification of covariance matrices using a riemannian-based kernel for BCI applications," *Neurocomputing*, vol. 112, pp. 172–178, Jul. 2013.

[30] M. R. Islam, T. Tanaka, and M. K. I. Molla, "Multiband tangent space mapping and feature selection for classification of EEG during motor imagery," *J. Neural Eng.*, vol. 15, no. 4, Aug. 2018, Art. no. 046021.

[31] N. Lu, T. Li, X. Ren, and H. Miao, "A deep learning scheme for motor imagery classification based on restricted Boltzmann machines," *IEEE Trans. Neural Syst. Rehabil. Eng.*, vol. 25, no. 6, pp. 566–576, Jun. 2017.

[32] Y. R. Tabar and U. Halici, "A novel deep learning approach for classification of EEG motor imagery signals," *J. Neural Eng.*, vol. 14, no. 1, Feb. 2017, Art. no. 016003.

[33] D. I. Shuman, S. K. Narang, P. Frossard, A. Ortega, and P. Vandergheynst, "The emerging field of signal processing on graphs: Extending high-dimensional data analysis to networks and other irregular domains," *IEEE Signal Process. Mag.*, vol. 30, no. 3, pp. 83–98, May 2013.

[34] A. Sandryhaila and J. M. F. Moura, "Discrete signal processing on graphs: Frequency analysis," *IEEE Trans. Signal Process.*, vol. 62, no. 12, pp. 3042–3054, Jun. 2014.

[35] V. Kalofolias, "How to learn a graph from smooth signals," in *Proc. Artif. Intell. Statist.*, 2016, pp. 920–929.

[36] L. Stankovic, M. Dakovic, and E. Sejdic, "Vertex-frequency analysis: A way to localize graph spectral components [lecture notes]," *IEEE Signal Process. Mag.*, vol. 34, no. 4, pp. 176–182, Jul. 2017.

[37] W. Huang, T. A. W. Bolton, J. D. Medaglia, D. S. Bassett, A. Ribeiro, and D. Van De Ville, "A graph signal processing perspective on functional brain imaging," *Proc. IEEE*, vol. 106, no. 5, pp. 868–885, May 2018.

[38] S. Atasoy, L. Roseman, M. Kaelen, M. L. Kringelbach, G. Deco, and R. L. Carhart-Harris, "Connectome-harmonic decomposition of human brain activity reveals dynamical repertoire re-organization under LSD," *Sci. Rep.*, vol. 7, no. 1, Dec. 2017, Art. no. 17661.

[39] P. C. Petrantonakis and I. Kompatsiaris, "Single-trial NIRS data classification for brain–computer interfaces using graph signal processing," *IEEE Trans. Neural Syst. Rehabil. Eng.*, vol. 26, no. 9, pp. 1700–1709, Sep. 2018.

[40] G. Kalantar, H. Sadreazami, A. Mohammadi, and A. Asif, "Adaptive dimensionality reduction method using graph-based spectral decomposition for motor imagery-based brain-computer interfaces," in *Proc. IEEE Global Conf. Signal Inf. Process. (GlobalSIP)*, Nov. 2017, pp. 990–994.

[41] K. Georgiadis, N. Laskaris, S. Nikolopoulos, and I. Kompatsiaris, "Connectivity steered graph Fourier transform for motor imagery BCI decoding," *J. Neural Eng.*, vol. 16, no. 5, Aug. 2019, Art. no. 056021.

[42] K. Georgiadis, N. Laskaris, S. Nikolopoulos, D. A. Adamos, and I. Kompatsiaris, "Using discriminative lasso to detect a graph Fourier transform (GFT) subspace for robust decoding in motor imagery BCI," in *Proc. 41st Annu. Int. Conf. IEEE Eng. Med. Biol. Soc. (EMBC)*, Jul. 2019, pp. 6167–6171.

[43] D. Slepian and H. O. Pollak, "Prolate spheroidal wave functions, Fourier analysis and uncertainty-I," *Bell Syst. Tech. J.*, vol. 40, no. 1, pp. 43–63, 1961.

[44] K. Georgiadis, D. A. Adamos, S. Nikolopoulos, N. Laskaris, and I. Kompatsiaris, "A graph-theoretic sensor-selection scheme for covariance-based motor imagery (MI) decoding," in *Proc. 28th Eur. Signal Process. Conf. (EUSIPCO)*, Jan. 2021, pp. 1234–1238.

[45] S. Nikolopoulos *et al.*, "A multimodal dataset for authoring and editing multimedia content: The MAMEM project," *Data Brief*, vol. 15, pp. 1048–1056, Dec. 2017.

[46] B. Blankertz *et al.*, "The BCI competition III: Validating alternative approaches to actual BCI problems," *IEEE Trans. Neural Syst. Rehabil. Eng.*, vol. 14, no. 2, pp. 153–159, Jun. 2006.

[47] D. Van De Ville, R. Demesmaeker, and M. G. Preti, "When slepian meets fiedler: Putting a focus on the graph spectrum," *IEEE Signal Process. Lett.*, vol. 24, no. 7, pp. 1001–1004, Jul. 2017.

[48] M. Petrovic, T. A. W. Bolton, M. G. Preti, R. Liégeois, and D. Van De Ville, "Guided graph spectral embedding: Application to the C. Elegans connectome," *Netw. Neurosci.*, vol. 3, no. 3, pp. 807–826, Jan. 2019.

[49] M. Pavan and M. Pelillo, "Dominant sets and pairwise clustering," *IEEE Trans. Pattern Anal. Mach. Intell.*, vol. 29, no. 1, pp. 167–172, Jan. 2007.

[50] D. A. Adamos, N. A. Laskaris, and S. Micheloyannis, "Harnessing functional segregation across brain rhythms as a means to detect EEG oscillatory multiplexing during music listening," *J. Neural Eng.*, vol. 15, no. 3, Jun. 2018, Art. no. 036012.

[51] M. X. Cohen, *Analyzing Neural Time Series Data: Theory and Practice*. Cambridge, MA, USA: MIT Press, 2014.

[52] F. Lotte *et al.*, "A review of classification algorithms for EEG-based brain–computer interfaces: A 10 year update," *J. Neural Eng.*, vol. 15, no. 3, Apr. 2018, Art. no. 031005.

[53] V. P. Oikonomou, K. Georgiadis, G. Liaros, S. Nikolopoulos, and I. Kompatsiaris, "A comparison study on EEG signal processing techniques using motor imagery EEG data," in *Proc. IEEE 30th Int. Symp. Comput.-Based Med. Syst. (CBMS)*, Jun. 2017, pp. 781–786.

[54] N. Laskaris, D. A. Adamos, and A. Bezerianos, "A tutorial on graph theory for brain signal analysis," 2020, *arXiv:2007.05800*. [Online]. Available: http://arxiv.org/abs/2007.05800